Geochemistry
Geophysics
Geosystems
$G^3$
AN ELECTRONIC JOURNAL OF THE EARTH SCIENCES
Published by AGU and the Geochemical Society

*Article*
Volume 9, Number 3
22 March 2008
Q03019, doi:10.1029/2007GC001920
ISSN: 1525-2027

# Gas hydrate dissociation in sediments: Pressure-temperature evolution

**Tae-Hyuk Kwon and Gye-Chun Cho**
*Department of Civil and Environmental Engineering, Korea Advanced Institute of Science and Technology (KAIST), Daejeon 305-701, South Korea (kikig@kaist.ac.kr; gyechun@kaist.edu)*

**J. Carlos Santamarina**
*School of Civil and Environmental Engineering, Georgia Institute of Technology, 790 Atlantic Drive, Atlanta, Georgia 30332, USA (jcs@gatech.edu)*

[1] Hydrate-bearing sediments may destabilize spontaneously as part of geological processes, unavoidably during petroleum drilling/production operations or intentionally as part of gas extraction from the hydrate itself. In all cases, high pore fluid pressure generation is anticipated during hydrate dissociation. A comprehensive formulation is derived for the prediction of fluid pressure evolution in hydrate-bearing sediments subjected to thermal stimulation without mass transfer. The formulation considers pressure- and temperature-dependent volume changes in all phases, effective stress-controlled sediment compressibility, capillarity, and the relative solubilities of fluids. Salient implications are explored through parametric studies. The model properly reproduces experimental data, including the PT evolution along the phase boundary during dissociation and the effect of capillarity. Pore fluid pressure generation is proportional to the initial hydrate fraction and the sediment bulk stiffness; is inversely proportional to the initial gas fraction and gas solubility; and is limited by changes in effective stress that cause the failure of the sediment. When the sediment stiffness is high, the generated pore pressure reflects thermal and pressure changes in water, hydrate, and mineral densities. Comparative analyses for $CO_2$ and $CH_4$ highlight the role of gas solubility in excess pore fluid pressure generation. Dissociation in small pores experiences melting point depression due to changes in water activity, and lower pore fluid pressure generation due to the higher gas pressure in small gas bubbles. Capillarity effects may be disregarded in silts and sands, when hydrates are present in nodules and lenses and when the sediment experiences hydraulic fracture.

**Components:** 6619 words, 8 figures, 4 tables.

**Keywords:** pressure evolution; excess pore pressure; gas hydrate; dissociation; self preservation; hydrate-bearing sediments.

**Index Terms:** 3004 Marine Geology and Geophysics: Gas and hydrate systems; 1012 Geochemistry: Reactions and phase equilibria (3612, 8412); 3021 Marine Geology and Geophysics: Marine hydrogeology.

**Received** 2 December 2007; **Revised** 22 January 2008; **Accepted** 4 February 2008; **Published** 22 March 2008.

Kwon, T.-H., G.-C. Cho, and J. C. Santamarina (2008), Gas hydrate dissociation in sediments: Pressure-temperature evolution, *Geochem. Geophys. Geosyst.*, *9*, Q03019, doi:10.1029/2007GC001920.

## 1. Introduction

[2] Hydrate-bearing sediments are found in continental margins and permafrost where pressure and temperature satisfy stability conditions. At the pore scale, hydrates exist in disseminated form in coarse-grained sediments, or are concentrated in nodules and lenses in fine-grained silty or clayey deposits [*Dillon and Max*, 2000].

[3] Hydrate-bearing sediments may destabilize spontaneously as part of geological processes, unavoidably during petroleum drilling/production operations [*Briaud and Chaouch*, 1997], or intentionally as part of gas extraction from the hydrate itself. Potential gas production methods include depressurization, inhibitor injection, thermal stimulation, and their combinations [*Holder et al.*, 1984; *Moridis*, 2003; *Pawar et al.*, 2005].

[4] High pore fluid pressure generation is anticipated during hydrate dissociation. One unit volume of methane hydrate $V_0$ dissociates at a constant pressure of 10 MPa to occupy a combined volume of 2.62 $V_0$ (where water and gas volumes are $V_W = 0.79\ V_0$ and $V_G = 1.83\ V_0$, respectively). Assuming the final pressure and temperature to be 1 atm and 20°C, the final combined volume would be 183.95 $V_0$ ($V_W = 0.79\ V_0$ and $V_G = 183.16\ V_0$). Such a large volume expansion would generate high fluid pressure and/or large fluid flux. Furthermore, the effective stress-dependent sediment stiffness, shear strength and fluid conduction would be affected by changes in the pore fluid pressure [*Briaud and Chaouch*, 1997; *Birchwood et al.*, 2005; *Nixon and Grozic*, 2007].

[5] Clearly, pressure generation depends on the initial volume fraction of the phases (including gas, e.g., at the base of the gas hydrate stability zone), the rates of fluid flow, heat flux, and the global volume change experienced by the hydrate-bearing sediment [*Ullerich et al.*, 1987; *Kayen and Lee*, 1991; *Sultan et al.*, 2004; *Xu and Germanovich*, 2006].

[6] Reliable predictions of gas production, pressure evolution and fluid flow are required in relation to any possible dissociation event. The purpose of this study is to derive a comprehensive formulation to predict the evolution of fluid pressure as a result of hydrate dissociation in sediments subjected to thermal stimulation. The formulation is extended to take into consideration sediment compressibility and capillary effects. It is then applied in a comparative analysis of methane and carbon dioxide hydrate bearing sediments. The manuscript starts with a discussion of concurrent events taking place during hydrate dissociation in sediments.

## 2. Underlying Processes

[7] Consider a mass of gas hydrate within the stability zone, away from the phase transformation boundary, subjected to a gradual increase in temperature. The following processes develop as temperature increases (refer to Figure 1).

### 2.1. Gas Solubility

[8] In the absence of hydrates, gas solubility in water increases as temperature decreases and pressure increases, as prescribed in Henry's law [*Lide*, 1997; *Osegovic et al.*, 2006]. The presence of hydrates facilitates further hydrate formation, and hence the equilibrium concentration of gas in water decreases and gas solubility in water increases with temperature [*Handa*, 1990; *Aya et al.*, 1997; *Davie et al.*, 2004; *Servio and Englezos*, 2001; *Duan and Mao*, 2006]; this observation applies to the A-B path in the stability "$H + L_w$" zone in Figure 1. Eventually, gas solubilities in water with and without hydrate converge at the phase boundary P-T. Accordingly, Henry's law applies along the B-C-D path in Figure 1.

### 2.2. Dissolution

[9] The increase in temperature within the stability zone (A to B in Figure 1) causes an initial breakdown of the hydrate structure due to the increased gas solubility in the surrounding pore water. "Hydrate dissolution" generates water and dissolved gas; there is no free gas produced. The relatively small pore pressure change that accompanies dissolution may be critical at shallow sediment depth below seafloor. [*Sultan et al.*, 2004; *Sultan*, 2007; *Xu and Germanovich*, 2007].

### 2.3. Dissociation

[10] Hydrate dissociation starts when the PT state reaches the equilibrium boundary (point B in Figure 1). During heating under restricted volume expansion, the PT state remains on the phase boundary until all hydrate dissociates (B to C in Figure 1; isochoric heating is the extreme case of constrained volume expansion). This response has been conveniently used to identify the phase boundary [*Marshall et al.*, 1964; *Schroeter et al.*, 1983]. Dissociation produces free gas, gas-saturated water, and water vapor saturated gas. The pro-

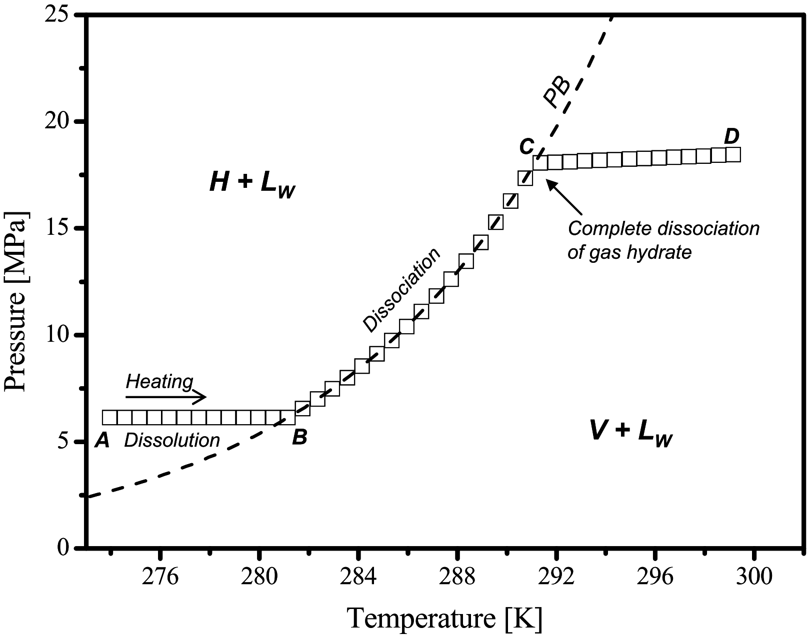

**Figure 1.** Pressure and temperature evolution during thermal stimulation. $L_W$, liquid water; $H$, hydrate; $V$, $CH_4$ in vapor phase. The phase boundary PB shown corresponds to pure methane hydrate in Table 1: $P$ [kPa] = exp (40.234–8860/T [K]); this expression is modified from *Sloan* [1998] using data computed with the HWHYD software (2001; a demo version of this software is available at http://www.pet.hw.ac.uk/research/hydrate).

nounced volume expansion during dissociation translates into high excess fluid pressure when fluid flow and sediment expansion are constrained. This situation develops when the rate of hydrate dissociation is faster than the rate of pore pressure dissipation and the expansion of the sediment is restricted by the stiffness of the surrounding medium.

[11] The dissociation rate is proportional to the specific surface area of the hydrate, to rate of heat transfer from the surroundings, and to the difference in fugacity between methane at the equilibrium pressure and at the decomposition pressure [*Kim et al.*, 1987; *Circone et al.*, 2005a].

## 2.4. Self Preservation

[12] The increase in pressure along the PT boundary during thermally driven dissociation under restricted or constrained volume expansion hinders further dissociation. The complementary effect takes place during dissociation under adiabatic conditions whereby the endothermic reaction leads to a decrease in temperature, which slows hydrate dissociation.

[13] In addition, if the temperature drops to the ice point, ice forms on the outer surface of dissociating hydrate further preserving the encapsulated hydrate phase. The ice shield is particularly effective between 240 K and 273 K at atmospheric pressure as the new hexagonal ice is able to anneal. This serves to heal defects and stacking faults, and gas transport is thereby severely diminished [*Stern et al.*, 2001; *Kuhs et al.*, 2004; *Circone et al.*, 2005a]. Isochoric, adiabatic and the ice-shield self preservation responses aid sample recovery from natural hydrate-bearing sediments in both standard and pressure coring operations, and may hinder methane production [e.g., see *Moridis and Sloan*, 2006].

## 2.5. Beyond Hydrate Dissociation

[14] Water (with dissolved gas), free gas (with water vapor), and the mineral phase remain once the gas hydrate has completely dissociated. Thereafter, an additional increase in temperature under limited or constrained volume expansion causes an increase in pressure, which is induced by the thermal expansion of the phases (C to D in Figure 1).

## 2.6. P- and T-Dependent Volume Change in the Phases

[15] Thermal and pressure induced volumetric strains take place in all components throughout the different stages of heating (A to B, B to C, and C to D).

## 2.7. P-Dependent Global Volume Change

[16] Excess pore pressure generation implies a decrease in effective stress and expansion of the sediment skeletal structure, i.e., an increase in the total volume of the sediment. Temperature itself has a very small effect on the skeletal volume.

## 2.8. Phase Boundary for Hydrate in Small Pores

[17] Water is thermodynamically preferred over the hydrate phase on mineral surfaces. Therefore, water wets the mineral surface at the hydrate-water interface and encloses the hydrate mass within a concave surface, which exerts an additional confinement $\Delta P = 2\gamma/r$ beyond the fluid pressure (where $\gamma$ is the interfacial tension between hydrate and water, and $r$ is the pore size in radius). The higher pressure in the hydrate mass does not mean stability to higher temperatures. On the contrary, the mineral preference for water prevails, water activity decreases, and there is a shift in the hydrate phase boundary toward lower temperatures, i.e., freezing/melting point depression, which is most noticeable in small pores (see data of *Uchida et al.* [2002] and *Anderson et al.* [2003b] and discussion by *Christenson* [2001]).

# 3. Analytical Formulation

[18] The evolution of the pore fluid pressure during gas hydrate dissociation in sediments is analyzed in detail next, taking into consideration the phenomena described above. We assume no fluid flux to explore the situation when the rate of dissociation is much faster than the rate of pore pressure generation. This condition is expected in various field situations, including the thermal stimulation of fine-grained sediments where the thermal diffusion coefficient is typically higher than the pressure diffusion coefficient (by one order of magnitude or more in high-plasticity clays).

[19] We relax some of the a-priori assumptions made in previous studies and seek to derive general expressions that facilitate identifying the interplay among various parameters and processes. In particular, we take into consideration dissolved gas, the stiffness of the sediment (related to sediment depth and effective stress), and the volume change in all phases as a function of temperature and pressure (parameters are listed in Table 1).

[20] Hydrate and water are in equilibrium without a free gas phase within the stability zone above the base of the stability zone [*Handa*, 1990; *Clennell et al.*, 1999]. However, water-limited conditions may be locally encountered in natural sediments subjected to high gas transport. Accordingly, the coexistence of free methane gas and gas hydrate has been reported in natural sediments, for example in the southern Hydrate Ridge [*Liu and Flemings*, 2006] and in the Nigerian continental slope [*Sultan et al.*, 2007]. Therefore, the generic formulation developed next includes all phases: gas, water, hydrate, and mineral.

## 3.1. Assumptions and Governing Equations

[21] The P- and T-dependent volume change in mineral, water, and hydrate phases is computed assuming an additive contribution of thermal and elastic deformations (Table 2):

$$\mathrm{dV} = \mathrm{dP}\left(\frac{\partial \mathrm{V}}{\partial \mathrm{P}}\right)_{\mathrm{T}} + \mathrm{dT}\left(\frac{\partial \mathrm{V}}{\partial \mathrm{T}}\right)_{\mathrm{P}} = \mathrm{dP}\left(-\frac{1}{\mathrm{B}}\cdot \mathrm{V}_0\right) + \mathrm{dT}(\mathrm{b}\cdot \mathrm{V}_0) \tag{1}$$

[22] The response of real materials for large P and T changes deviates from the additive rule; however, this simple assumption helps identify their separate contributions. Alternatively, empirically determined $\rho = f(P, T)$ functions can be used. Note that there is partial cancellation between thermal expansion and elastic contraction of the phases during thermal stimulation.

[23] The pore water is assumed to be gas saturated, and the solubility of gas in water is computed using Henry's law. We disregard the solubility of water vapor in gas (the water vapor pressure is much smaller than the methane gas pressure), and the density change of water due to the dissolved gas.

[24] The mass of each species is conserved within the boundaries during the thermal stimulation of the hydrate-bearing sediments, i.e., zero fluid flux assumption. In particular, the total mass of hydrate-forming gas (HFG) remains constant:

$$\begin{aligned} &\text{Initial} && n^{HFG} = n_{h0}^{HFG} + n_{aq0}^{HFG} + n_{g0}^{HFG} \\ &\text{After some dissociation} && \phantom{n^{HFG}} = n_{h}^{HFG} + n_{aq}^{HFG} + n_{g}^{HFG} \end{aligned} \tag{2}$$

[25] The moles of hydrate-forming gas $n^{HFG}$ in each phase are captured using expressions listed in Table 3.

**Table 1.** Parameters Used in This Study

| Parameter | Definition, Dimension | Values Selected for This Study |
|---|---|---|
| $B$ | Bulk modulus, GPa | |
| $B_h$ | of gas hydrate | 5.6 for methane hydrate[a] |
| $B_w$ | of water | 2[b] |
| $B_m$ | of minerals | 67 for quartz[b] |
| $B_{sk}$ | of sediments | - |
| $d$ | Pore size in diameter, m | |
| $\Delta H_{solution}$ | Enthalpy of the solution, J $mol^{-1}$ | −39580 for $CH_4$[c] and −19960 for $CO_2$[d] |
| $k_H^T$ | Gas solubility at temperature $T$ (Henry's law), mol $L^{-1}$ $atm^{-1}$ | $k_H{}^T = k_H{}^o \cdot \exp\left[\frac{-\Delta H_{solution}}{R}\left(\frac{1}{T} - \frac{1}{T_{298.15K}}\right)\right]$ |
| $k_H^o$ | Henry's constant at 298 K, mol $m^{-3}$ $atm^{-1}$ | 0.599 for $CH_4$[c] and 35 for $CO_2$[d] |
| $L_f$ | Latent heat of dissociation, kJ $mol^{-1}$ | 53.2 [e] for methane hydrate |
| $m$ | Molecular weight, g $mol^{-1}$ | |
| $m_h$ | of gas hydrate (= $m_{gas} + \chi\, m_w$) | 119.5 for $CH_4 \cdot 5.75H_2O$ |
| $m_w$ | of water | 18 |
| $n^{HFG}$ | Mole of hydrate-forming gas, mole | |
| $n_h$ | in hydrate phase | |
| $n_{aq}$ | in aqueous phase | |
| $n_g$ | in gas phase | |
| $P$ | Fluid pressure: gas or water, Pa | |
| $P_{eq}^T$ | Equilibrium pressure on the hydrate stability boundary at temperature $T$ | $P_{eq}{}^T$[kPa] = exp ($a + b/T$ [K])<br>$a = 40.234$, $b = -8860$ for $CH_4$[f]<br>$a = 41.235$, $b = -9317$ for $CO_2$[f] |
| $R$ | Gas constant, J $mol^{-1}$ $K^{-1}$ | 8.315 |
| $R_m$ | Molar mass ratio of hydrate-forming gas to gas hydrate, dimensionless | $R_m = \frac{\text{molar mass of hydrate-forming gas}}{\text{molar mass of gas hydrate}}$<br>For methane hydrate, $R_m = 0.134$ for hydration number $\chi = 5.75$. |
| $S$ | Volume fraction in pores, dimensionless | $S_{h0} + S_{w0} + S_{g0} = 1$ |
| $S_h$ | of gas hydrate | $S_{h0} = V_{h0}/V_{p0}$ |
| $S_w$ | of water | $S_{w0} = V_{w0}/V_{p0}$ |
| $S_g$ | of free gas | $S_{g0} = V_{g0}/V_{p0}$ |
| $T$ | Absolute temperature, K | |
| $V$ | Volume, $m^3$ | |
| $\beta$ | Thermal expansivity, $K^{-1}$ | $\Delta V = \beta\, \Delta T V_0$ |
| $\beta_h$ | of gas hydrate | $2.57 \times 10^{-5}$ for methane hydrate[a] |
| $\beta_w$ | of water | $2.0 \times 10^{-4}$[b] |
| $\beta_m$ | of minerals | $2.1 \times 10^{-4}$[b] |
| $\gamma$ | Surface tension, N/m | $\gamma_{hw} = 0.032$[e] for water-hydrate interface<br>$\gamma_{gw} = 0.072$[d,g] for water-gas interface |
| $\varepsilon$ | Volumetric strain, dimensionless | |
| $\phi$ | Porosity of the sediment, dimensionless | |
| $\rho$ | Mass density, kg $m^{-3}$ | |
| $\rho_h$ | of gas hydrate | 910 for methane hydrate[a] |
| $\rho_w$ | of water | 998 for pure water[b] |
| $\chi$ | Hydration number, dimensionless | 5.75 for methane hydrate[a] |

[a] *Sloan* [1998].
[b] *Santamarina et al.* [2001].
[c] The solubility coefficients for methane are modified using data from *Duan and Mao* [2006].
[d] *Lide* [1997].
[e] *Anderson et al* [2003b].
[f] The expressions for the phase boundary of methane hydrate and $CO_2$ hydrate from *Sloan* [1998] are modified using data computed with the HWHYD software [2001].
[g] *Clennell et al.* [1999].

[26] The total volumetric expansion of the hydrate-bearing sediment is the sum of the volume change experienced by each constituent, and is equal to the volume expansion of the granular skeleton against the surrounding medium, associated with the increase in pore fluid pressure. As the effective stress $\sigma' = \sigma_{tot} - P$, the change in effective stress for a

**Table 2.** Density as a Function of Temperature and Pressure

| Phase | Initial Density (at $P_0$ and $T_0$) | Density (at $P$ and $T$) | Volumetric Strain |
|---|---|---|---|
| Mineral | $\rho_{m0}$ | $\rho_m = \frac{\rho_{m0}}{1+\varepsilon_m}$ | $\varepsilon_m = -\frac{\Delta P}{B_m} + \beta_m \Delta T$ |
| Hydrate | $\rho_{h0}$ | $\rho_h = \frac{\rho_{h0}}{1+\varepsilon_h}$ | $\varepsilon_m = -\frac{\Delta P}{B_h} + \beta_h \Delta T$ |
| Water | $\rho_{w0}$ | $\rho_w = \frac{\rho_{w0}}{1+\varepsilon_w}$ | $\varepsilon_w = -\frac{\Delta P}{B_w} + \beta_w \Delta T$ |

constant overburden is $-\Delta\sigma' = \Delta P$; then the volumetric strain is

$$\begin{aligned} \varepsilon &= \frac{-\Delta\sigma'}{B_{sk}} = \frac{\Delta V_t}{V_{t0}} \\ &= \frac{\Delta P}{B_{sk}} = \frac{\Delta V_m}{V_{t0}} + \frac{\Delta V_h}{V_{t0}} + \frac{\Delta V_w}{V_{t0}} + \frac{\Delta V_g}{V_{t0}} \end{aligned} \tag{3}$$

## 3.2. Conditions Before and After Partial Dissociation

[27] The sediment has an initial porosity $\phi = V_{pore}/V_{t0}$. The hydrate phase is in equilibrium before heating ($P_0 = P_{eq}^{T0}$, $T_0$), and it occupies a pore volume fraction $S_{h0}$; water $S_{w0}$ and free gas $S_{g0}$ fill the rest of the pore volume so that $S_{h0} + S_{w0} + S_{g0} = 1$. The initial volume of each phase is expressed as a function of volume fractions in Table 4.

[28] Gas hydrate partially dissociates during heating (i.e., $-\Delta M_h$, $T = T_0 + \Delta T$), contributing both water to the water phase and gas to the gas phase (note that the sign of $\Delta M_h$ is negative during dissociation). The final volume and corresponding volume change for each phase after partial dissociation are given in Table 4. Initial and final masses are summarized in Table 4.

## 3.3. General Equation

[29] Expressions in Table 4 are substituted into equation (3) to obtain a general expression:

$$\begin{aligned} \varepsilon = (1-\phi)\varepsilon_m + \phi(S_{h0}\varepsilon_h + S_{w0}\varepsilon_w) \\ + \frac{\Delta M_h}{V_{t0}}\left[\frac{1+\varepsilon_h}{\rho_{h0}} - \frac{(1+\varepsilon_w)(1-R_m)}{\rho_{w0}}\right] + \frac{\Delta V_g}{V_{t0}} \end{aligned} \tag{4}$$

[30] The last term $\Delta V_g/V_{t0}$ is the volume change of gas normalized by the initial volume of the hydrate-bearing sediment. It can be expressed as follows:

$$\frac{\Delta V_g}{V_{t0}} = \frac{n_g^{HFG} RT}{PV_{t0}} - \phi \cdot S_{g0} \tag{5}$$

[31] Then, we replace $n_g^{HFG}$ by equations in Table 3 to obtain

$$\begin{aligned} \frac{\Delta V_g}{V_{t0}} = \frac{\Delta M_h}{V_{t0}} RT\left[(1+\varepsilon_w)k_H^T \frac{1-R_m}{\rho_{w0}} - \frac{1}{m_h P}\right] \\ + \phi S_{w0} RT\left[k_H^{T_0}\frac{P_0}{P} - (1+\varepsilon_w)k_H^T\right] \\ + \phi S_{g0}\left(\frac{T}{T_0}\frac{P_0}{P} - 1\right) \end{aligned} \tag{6}$$

[32] As long as hydrate remains in the system, the pressure $P$ for a given temperature $T$ is the corresponding equilibrium pressure $P_{eq}^T$ on the phase boundary. The increase in pressure $\Delta P_{final}$ when all the hydrate in the system is consumed can be evaluated using equations (4)–(6) for $\Delta M_h = -M_{h0}$.

## 3.4. Volumetric Fractions During Thermal Stimulation

[33] Volumetric and gravimetric quantities of any phase can be evaluated using the equations in Table 4, including the molar quantity of methane in the gas phase or the volume fraction of free gas in pores. These quantities help assess the evolution of

**Table 3.** Hydrate-Forming Gas Content in Each Phase Before and After Dissociation[a]

| Phase | Before Dissociation (at $P_0$ and $T_0$) | After Partial Dissociation (at $P$ and $T$) |
|---|---|---|
| Hydrate phase | $n_{h0}^{HFG} = \frac{M_{h0}}{m_h}$ | $n_h^{HFG} = \frac{M_{h0}+\Delta M_h}{m_h}$ |
| Aqueous phase | $n_{aq0}^{HFG} = k_H^{T_0} \cdot P_0 \cdot V_{w0}$ | $n_{aq}^{HFG} = k_H^T \cdot P \cdot V_w$ |
| Gas phase | $n_{g0}^{HFG} = \frac{P_0 \cdot V_{g0}}{R \cdot T_0}$ | $n_g^{HFG}$ from mass conservation:<br>$0 = n_{h0}^{HFG} + n_{g0}^{HFG} + n_{aq0}^{HFG}$<br>$- n_h^{HFG} - n_g^{HFG} - n_{aq}^{HFG}$ |

[a] HFG, hydrate-forming gas. Content in moles. Note that the P-T state falls on the phase equilibrium after partial dissociation, i.e., $P_0 = P_{eq}^{T_0}$, and $P = P_{eq}^T$.

**Table 4.** Volume, Volume Change, and Mass Before and After Partial Dissociation[a]

| Phase | Initial Volume (at $P_0$ and $T_0$) | Volume After Partial Dissociation (at $P$ and $T$) | Volume Change From ($P_0$, $T_0$) to ($P$, $T$) | Initial Mass (at $P_0$ and $T_0$) | Mass After Partial Dissociation (at $P$ and $T$) |
|---|---|---|---|---|---|
| Mineral | $V_{m0} = (1 - \phi) \cdot V_{t0}$ | $V_m = \frac{M_{m0}}{\rho_m}$ | $\Delta V_m = (1 - \phi) \cdot V_{t0} \cdot \varepsilon_m$ | $M_{m0} = (1 - \phi) \cdot V_{t0} \cdot \rho_{m0}$ | $M_m = M_{m0}$ |
| Hydrate | $V_{h0} = \phi \cdot S_{h0} \cdot V_{t0}$ | $V_h = \frac{M_{h0}+\Delta M_h}{\rho_h}$ | $\Delta V_h = \phi \cdot S_{h0} V_{t0} \cdot \varepsilon_h + \frac{\Delta M_h}{\rho_{h0}} (1 + \varepsilon_h)$ | $M_{h0} = \phi \cdot S_{h0} \cdot V_{t0} \cdot \rho_{h0}$ | $M_h = M_{h0} + \Delta M_h$ |
| Water | $V_{w0} = \phi \cdot (1 - S_{h0} - S_{g0}) \cdot V_{t0}$ | $V_w = \frac{M_{w0}-\Delta M_h(1-R_m)}{\rho_w}$ | $\Delta V_w = \phi \cdot (1 - S_{h0} - S_{g0}) \cdot V_{t0} \cdot \varepsilon_w - \frac{\Delta M_h}{\rho_{w0}} \cdot (1 + \varepsilon_w) \cdot (1 - R_m)$ | $M_{w0} = \phi \cdot (1 - S_{h0} - S_{g0}) \cdot V_{t0} \cdot \rho_{w0}$ | $M_w = M_{w0} - \Delta M_h \cdot (1 - R_m)$ |
| Gas | $V_{g0} = \phi \cdot S_{g0} \cdot V_{t0}$ | $V_g = \frac{n_g^{HFG} RT}{P}$ | $\Delta V_g = \frac{n_g^{HFG} RT}{P} - \phi \cdot S_{g0} \cdot V_{t0}$ | | |

[a] Note that the P-T state falls on the phase equilibrium after partial dissociation, i.e., $P_0 = P_{eq}^{T_0}$, and $P = P_{eq}^{T}$.

the system during dissociation: gas will flow when the volume fraction of free gas $S_g$ exceeds the gas percolation threshold (typically $S_g > 0.2$ to 0.3), and limited water flow should be expected thereafter, leaving a residual water saturation that may exceed $S_w = 0.4$.

[34] Of particular interest is the hydrate mass change $\Delta\ M_h$ during dissociation (BC path in Figure 1). It can be computed using equations (4)–(6) for a given PT state on the phase boundary ($P_{eq}^T$, $T$). The remaining gas hydrate volume fraction $S_h$ is related to $\Delta M_h$ through the mass density, with proper consideration of volumetric strains

$$S_h(\Delta M_h) = \frac{\left(\phi \cdot S_{h0} + \frac{\Delta M_h}{\rho_{h0} V_{t0}}\right)(1 + \varepsilon_h)}{\left(1 + \frac{\Delta P}{B_{sk}}\right) - (1 - \phi)(1 + \varepsilon_m)} \qquad (7)$$

# 4. Discussion: Implications

## 4.1. Initial Hydrate and Gas Fractions

[35] Thermal stimulation of hydrate-bearing sediments under undrained conditions can cause a very large increase in the fluid pressure (i.e., several megapascals) when volume expansion is restricted by the high skeletal stiffness $B_{sk}$ of the medium. Numerical results in Figure 2 show that the excess fluid pressure during partial dissociation is primarily determined by the increase in temperature, while the excess fluid pressure after complete dissociation is strongly dependent on the initial volume fractions of hydrate $S_{h0}$ and free gas $S_{g0}$. The generated pore pressure is inversely proportional to the hydration number $\chi$ (Note that all results shown in this manuscript were computed assuming the stoichiometric $\chi = 5.75$. A hydration number $\chi = 6$ is typically encountered in natural hydrates [*Circone et al.*, 2005b].).

[36] The existence of a gas phase acts as a cushion against the pressure increase, diminishes self preservation and allows for faster gas hydrate dissociation with increasing temperature (Figure 2b). In the absence of fluid flux, a significantly high increase in temperature would be required to attain complete dissociation. For example, a 12°C increase in temperature is needed to completely dissociate a 40% volume fraction of methane hydrate (a lower temperature increase will suffice to dissociate the same amount in gassy or soft sediments).

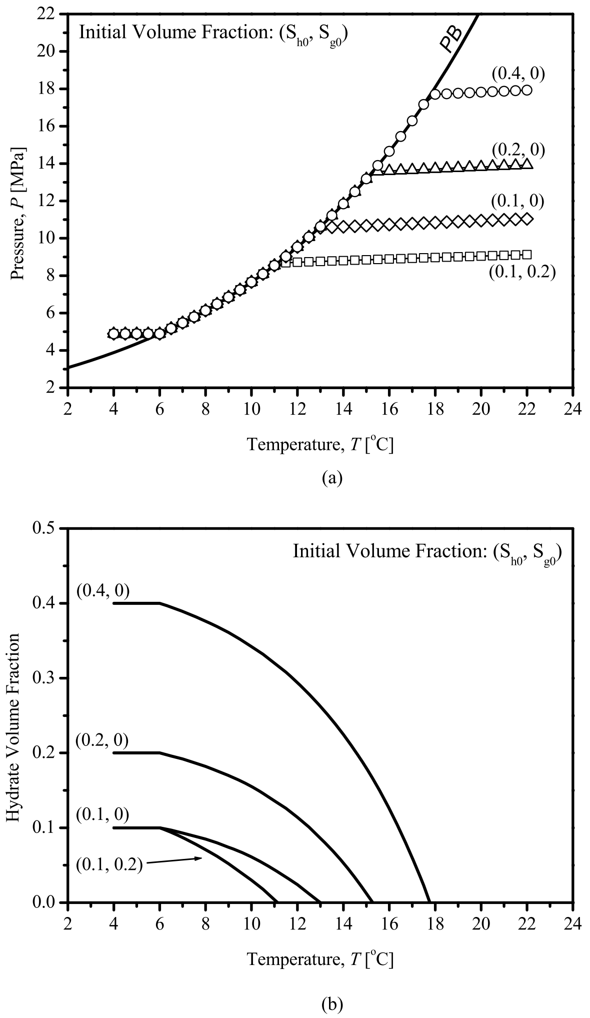

(a)

(b)

**Figure 2.** Thermal stimulation of methane hydrate-bearing sediments. Initial conditions: $T$ = 4°C, $P$ = 4.9 MPa, and sediment stiffness $B_{sk}$ = 100 MPa. (a) Pressure evolution. (b) Change in hydrate volume fraction. Dissociation begins at temperature of 6°C. Note that PB represents the phase boundary of pure methane hydrate in Table 1: $P$ [kPa] = exp(40.234−8860/T [K]); this expression is modified from *Sloan* [1998] using data computed with the HWHYD software (2001).

[37] Experimental data were gathered with a transparent reaction cell (volume 3.17 $cm^3$; internal diameter 6.35 mm; height 100 mm) packed with water saturated sand at a porosity $\phi$ = 0.4 (Ottawa F110; uniform grain size; mean diameter = 0.1 mm). Water and $CO_2$ gas were sequentially flushed through the specimen (P = 3.2 MPa and T = 2°C) and left to form gas hydrate and to stabilize for 3 days. Then, the cell was slowly heated at 0.5°C/h without allowing fluid flux. The measured temperature-pressure data are shown in Figure 3 for two tests (the initial pressure and temperature conditions were 3.4 MPa and 4°C for Test1; and 3.9 MPa and 5°C for Test 2). Trends show clear self preservation response along the phase boundary. Test 1 data were fitted with the analytical solution to infer the initial volume fractions in the system: $S_{h0}$ = 5%, $S_{w0}$ = 16%, $S_{g0}$ = 79%. The high pressure that develops during hydrate dissociation can cause liquefaction of $CO_2$; Test 2 demonstrates this situation (Figure 3). The model can be extended to accommodate gas liquefaction by taking into consideration the mass balance equations within the proper phase boundary.

## 4.2. Effective Stress and Sediment Stiffness: Depth Effect

[38] The stiffness of uncemented sediments is determined by the effective stress $B_{sk} = \alpha(\sigma')^{\beta}$ [*Santamarina et al.*, 2001]. Accordingly, low-stiffness shallow sediments will experience larger volumetric deformation and lower excess pore pressure than the same sediments at greater depth, as shown in Figure 4. Still, high excess fluid pressures are anticipated.

[39] Eventually, the fluid pressure is limited by the effective stress-dependent sediment strength. The dashed and dashed-dotted lines superimposed on Figure 4 indicate the extent of dissociation when the excess pore pressure equals the initial effective stress, i.e., "soil liquefaction." Low initial effective stress corresponds to low skeletal stiffness and decreased pore pressure generation during dissociation; however, it also implies low pore pressure required to reach failure.

[40] These results show that sediments may fail with a relatively low amount of hydrate dissociation. In fact, uncemented sediments in the upper 1000 mbsf may reach failure conditions with less than 6% hydrate dissociation in the absence of a gas phase and fluid flux.

[41] Nonplastic silts and sands (e.g., mean particle size > 10 $\mu$m, and specific surface < 1 $m^2/g$) develop higher bulk stiffness than plastic clayey soils (e.g., mean particle size < 1 $\mu$m, and specific surface > 1 $m^2/g$) at the same effective stress. Therefore, sandy soils could reach failure conditions before clayey sediments during thermal stimulation under zero fluid flow conditions. However, the higher hydraulic conductivity in sands will prevail in most field situations.

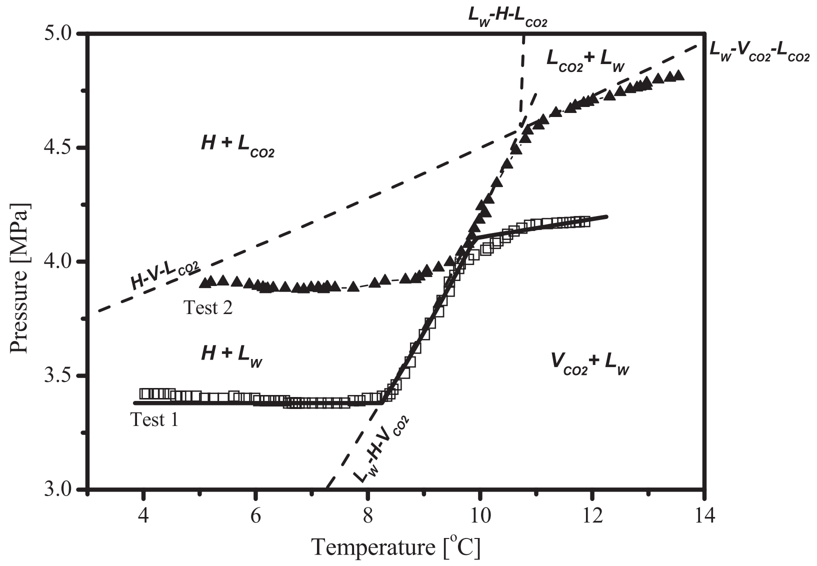

**Figure 3.** Measured pressure-temperature response during isochoric heating of $CO_2$ hydrate. The solid line represents the theoretical prediction curve for Test 1. $L_W$, liquid water, $H$, hydrate, $V_{CO2}$, $CO_2$ in vapor phase; $L_{CO2}$, $CO_2$ in liquid phase. The phase boundaries $L_W{-}H{-}V_{CO2}$, $H{-}V{-}L_{CO2}$, $L_W{-}V_{CO2}{-}L_{CO2}$, and $L_W{-}H{-}V_{CO2}$ are computed using the HWHYD software (2001).

### 4.3. Shallow Sediments: Simplification

[42] Low sediment stiffness in shallow formations and partial cancellation between thermal expansion and elastic contraction of the phases during thermal stimulation can be invoked to obtain the following simplified form of equation (4):

$$\varepsilon = \frac{\Delta M_h}{V_{t0}}\left[\frac{1}{\rho_{h0}} - \frac{1-R_m}{\rho_{w0}}\right] + \frac{\Delta V_g}{V_{t0}} \qquad (8)$$

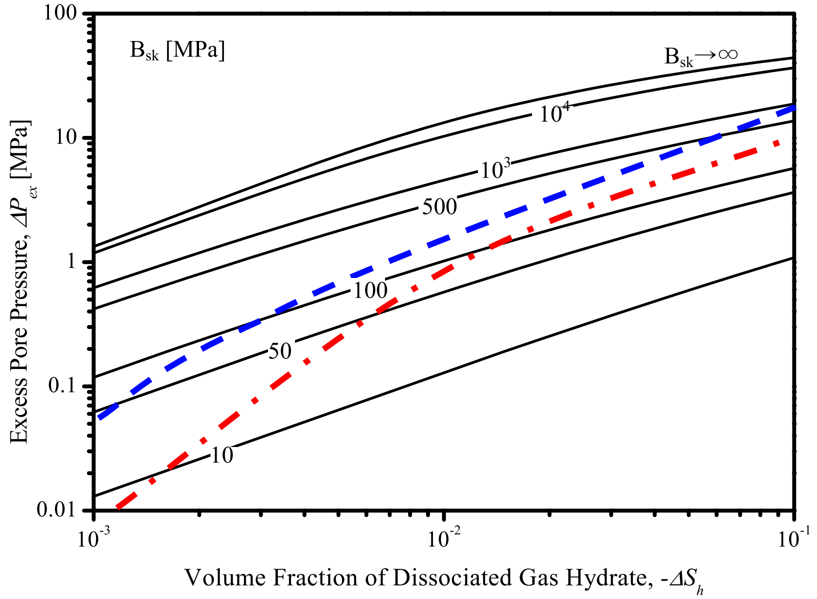

**Figure 4.** The effect of the sediments' stiffness on pressure evolution during the thermal stimulation of methane hydrate-bearing sediments. Initial conditions at the beginning of dissociation: $T = 6°C$, $P = 4.9$ MPa, initial hydrate fraction $S_{h0} = 20\%$, and initial gas fraction $S_{g0} = 0\%$. The dashed and dashed-dotted lines show sediment failure conditions (excess pore pressure equal to the initial effective stress): the blue dashed line applies to nonplastic sandy soils, and the red dashed-dotted line refers to high-plasticity clayey soils. All cases computed using values listed in Table 1.

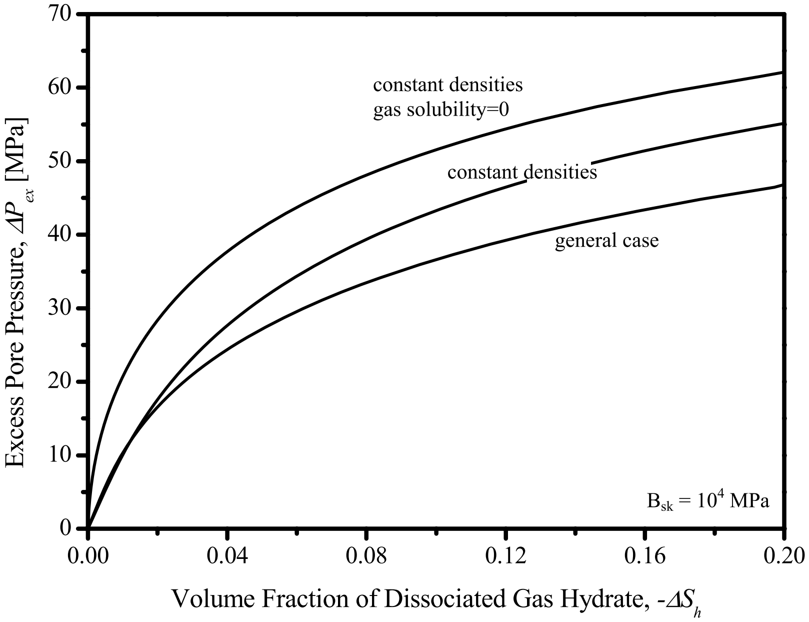

**Figure 5.** The effects of density changes in components and gas dissolution on pressure evolution during the thermal stimulation of methane hydrate-bearing sediments in stiff formations ($B_{sk}$ = $10^4$ MPa). Case "constant densities and gas solubility = 0" corresponds to the assumptions made by *Xu and Germanovich* [2006]. All cases computed using values listed in Table 1. Initial conditions at the beginning of dissociation: $T = 6°\mathrm{C}$, $P = 4.9$ MPa, initial hydrate fraction $S_{h0} = 20\%$, and initial gas fraction $S_{g0} = 0\%$.

[43] As a general guideline, this simplification is valid when the sediment bulk stiffness is $B_{sk} < 1$ GPa, which typically includes uncemented sediments in the upper 1000 mbsf.

## 4.4. Changes in Density

[44] Pore pressure generation is affected by density changes in the components in stiff formations with high hydrate volume fraction, as shown in Figure 5 (i.e., $B_{sk} > 1$ GPa). Otherwise, the simplified equation (8) applies.

## 4.5. Dissolved Gas

[45] The solubility of gas in water can have a distinct effect on excess pore pressure generation in stiff systems (Figure 5). The effect of gas solubility in water is highlighted by comparing the excess pore pressure produced by the dissociation of carbon dioxide $CO_2$ and methane hydrates (Figure 6) (note that $CO_2$ is ~10 times more soluble in water than $CH_4$). The reduction in excess fluid pressure generation by gas dissolution in water should not be disregarded a priori for all applications. In particular, the dissociation of $CO_2$ hydrate may produce less than one-third the excess pore pressure generated by $CH_4$ hydrate dissociation. Therefore, the more general equations are needed when considering other gases in related applications, such as $CO_2$ in sequestration and storage considerations.

## 4.6. Pore Size: Capillarity

[46] Capillarity in fine-grained sediments manifests itself through two mechanisms: freezing-melting point depression and increased gas pressure. First, the melting point depression $\Delta T_{dep}$ from the equilibrium temperature in unconfined conditions $T_{bulk}$ is computed using the Gibbs-Thomson equation with consideration of the total curvature of the solid surface in terms of the effective pore size $d$ [*Everett*, 1961; *Williams and Smith*, 1989; *Jallut et al.*, 1992; *Anderson et al.*, 2003a].

$$\text{Cylindrical hydrate shape} \quad \Delta T_{dep} = -\frac{2}{d}\left(\frac{\gamma_{hw} m_h \cos\theta}{\rho_{h0} L_f}\right) T_{bulk} \tag{9a}$$

$$\text{Spherical hydrate shape} \quad \Delta T_{dep} = -\frac{4}{d}\left(\frac{\gamma_{hw} m_h \cos\theta}{\rho_{h0} L_f}\right) T_{bulk} \tag{9b}$$

where $L_f$ is the latent heat of dissociation of gas hydrate (53.2 kJ/mol from *Anderson et al.* [2003b]), and $\gamma_{hw}$ is the surface tension between methane hydrate and water (~0.032 N/m after

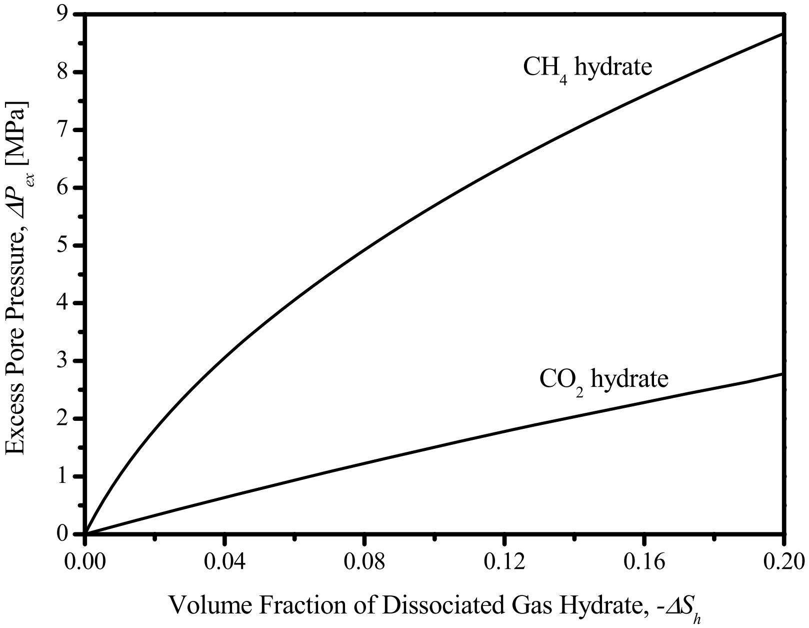

**Figure 6.** Dissociation of $CH_4$ and $CO_2$ hydrates. Initial conditions: sediment stiffness $B_{sk}$ = 100 MPa, initial hydrate fraction $S_{h0}$ = 20%, initial gas fraction $S_{g0}$ = 0%, initial temperature $T$ = 6°C, and the initial equilibrium pressure for $CH_4$ hydrate $P_{CH4}$ = 4.9 MPa and for $CO_2$ hydrate $P_{CO2}$ = 2.6 MPa.

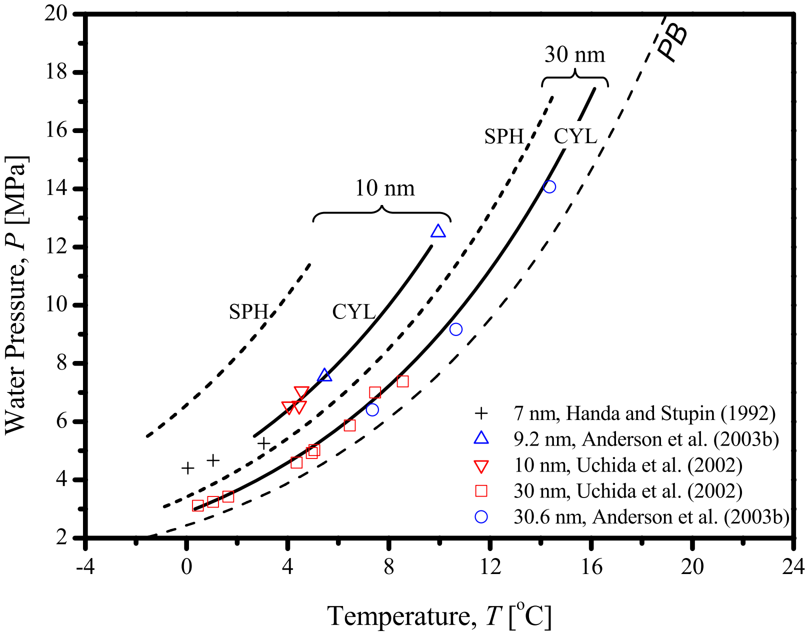

**Figure 7.** Capillary effects on phase boundary: Pore size and pore geometry. Published data and simulations. Initial conditions: sediment stiffness $B_{sk}$ = 100 MPa, initial hydrate fraction $S_{h0}$ = 80%, initial gas fraction $S_{g0}$ = 0%, and initial fluid pressure at the beginning of dissociation $P$ = 5.5 MPa for pore size $d$ = 10 nm and $P$ = 3.0 MPa for pore size $d$ = 30 nm. Note that the phase boundary PB shown corresponds to pure methane hydrate in unconfined sediments in Table 1: $P$ [kPa] = exp (40.234–8860/T [K]); this expression is modified from *Sloan* [1998] using data computed with the HWHYD software (2001).

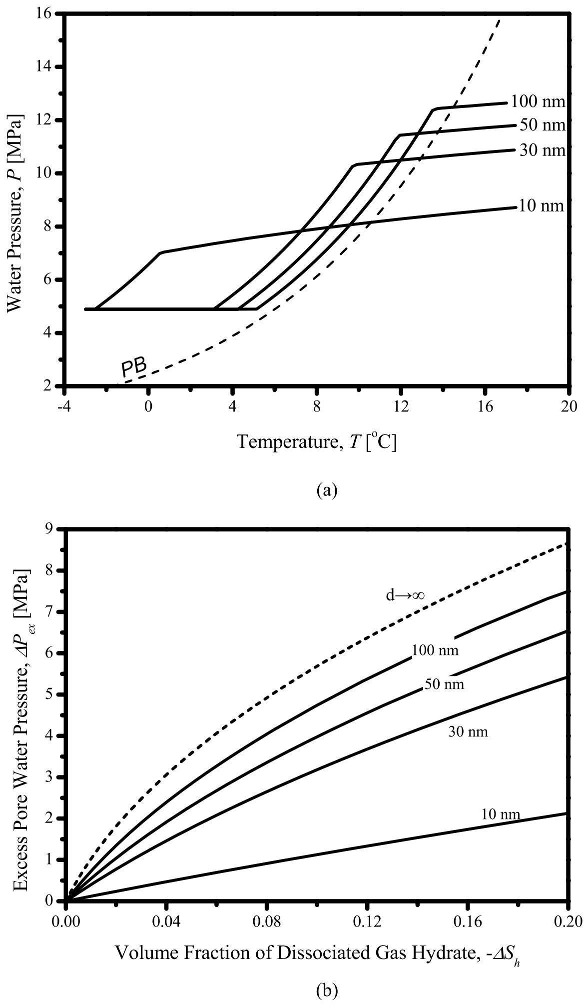

**Figure 8.** Effect of pore size on pore pressure generation. Initial conditions: sediment stiffness $B_{sk}$ = 100 MPa, initial hydrate fraction $S_{h0}$ = 20%, initial gas fraction $S_{g0}$ = 0%, initial temperature $T = -3$°C, and the initial fluid pressure $P$ = 4.9 MPa. (a) Pressure-temperature trace in PT plane. (b) Pressure evolution during dissociation. Note that the phase boundary PB shown corresponds to pure methane hydrate in unconfined sediments in Table 1: $P$ [kPa] = exp (40.234−8860/T [K]); this expression is modified from *Sloan* [1998] using data computed with the HWHYD software (2001).

*Uchida et al.* [1999] and *Anderson et al.* [2003b] and for ice in the work of *Clennell et al.* [1999]). Capillary effects on excess pore pressure generation along the phase boundary are shown in Figure 7, where the analytical solution is superimposed on previously published experimental data (we disregard changes in pore size during dissociation and consider the contact angle between the water and the pore wall to be $\theta = 0$ by assuming that minerals are coated by a water film). The results suggest that the hydrate surface can be presumed to be cylindrical when gas hydrate occupies most of the pore space (solid lines denoted as CYL in Figure 7). On the other hand, disseminated gas hydrate crystals may be encapsulated by spherical water films and experience higher capillary pressure and melting point depression (dashed lines denoted as SPH in Figure 7). Therefore, the dissociation temperature for a given pore size is affected by the hydrate fraction.

[47] Second, the increase in gas pressure inside spherical bubbles $P_g$ relative to the surrounding water pressure $P_w$ is computed using Laplace's equation to take into consideration the additional confinement exerted by the surface tension between gas and water $\gamma_{gw}$,

$$P_g = P_w + \frac{2\gamma_{gw}}{r} = P_w + \frac{4\gamma_{gw}}{d} \qquad (10)$$

[48] Figure 8 shows the pressure and temperature evolution of disseminated gas hydrate with 20% of hydrate fraction in pores. The water pressure evolves along the shifted phase boundary (Figure 8a). The pressure at the end of dissociation decreases in finer sediments due to the smaller volume occupied by the gas phase subjected to higher pressures in small bubbles (Figure 8b).

[49] The effects of pore size on melting point depression and pressure reduction vanish as pores exceed ~100 nm. Therefore, sands, silts and even kaolinites do not experience capillary effects. On the other hand, one should expect pronounced capillary effects in very fine clays, such as illite and montmorillonite, where the excess pore pressure may be as low as half the value of that in sands. However, capillary effects will vanish when hydrates are found in nodules, veins, and lenses, and when the high excess pore pressure causes the hydraulic fracture of the sediment, which is associated with a large increase in local pore size.

## 5. Conclusions

[50] A comprehensive analytical solution was derived to explore the evolution of hydrate-bearing sediments during thermal stimulation, with an emphasis on excess pore pressure generation under restricted or constrained volume conditions in the absence of fluid flux. The formulation captures the effects of sediment stiffness, the cushioning effect of an initial gas phase, change in the density of the phases, variation in gas solubility, the relevance of initial hydrate content, and capillary effects. The most important findings are as follows:

[51] 1. Partial dissociation during thermal stimulation is characterized by a pressure-temperature evolution along the phase boundary until all hydrate has dissociated. Higher gas hydrate concentration causes higher fluid pressure generation during dissociation and extends self preservation behavior during thermal stimulation. In addition to fluid flux, the presence of a gas phase, low skeletal stiffness and capillary effects reduce pressure generation.

[52] 2. Eventually, excess fluid pressure generation is limited by failure conditions. For a given hydrate concentration, lower excess pore pressure generation develops in shallow sediments due to lower sediment stiffness. However, shallower sediments require lower amounts of hydrate dissociation to reach failure than do deeper sediments, and hence they need a smaller increase in temperature. Less than 6% volume fraction dissociation may be sufficient to cause the failure of uncemented sediments in the upper 1000 mbsf, in the absence of fluid flux.

[53] 3. Thermal and pressure induced density changes in water, hydrate, and mineral can be disregarded in most applications (uncemented sediments in the upper 1000 mbsf), except in deep sediments with high initial stiffness.

[54] 4. Gas solubility in water diminishes pore pressure generation. The reduction in excess fluid pressure generation by gas dissolution in water should not be disregarded a priori for all applications. For example, the dissociation of $CO_2$ hydrate may produce less than one-third the excess pressure that is generated by $CH_4$ hydrate dissociation.

[55] 5. Hydrate dissociation in small pores is affected by melting point depression and lower fluid pressure generation due to the additional confinement the water-gas interface exerts on small gas bubbles. Therefore, lower excess pore water pressure develops in finer sediments with disseminated hydrates. Capillary effects vanish when pores exceed ~100 nm (sands and silts), when hydrates are present in nodules and lenses, and after the development of hydraulic fractures.

## Acknowledgments

[56] We are grateful to N. Sultan, W. Waite, C. Ruppel, and P. Taboada-Serrano for valuable comments and suggestions. Support for this research was provided by the Basic Research Program of the Korea Science & Engineering Foundation (KOSEF; grant R01-2006-000-10727-0) and the DOE Joint Industry Project for Methane Hydrate administered by Chevron.

## References

Anderson, R., M. Llamedo, B. Tohidi, and R. W. Burgass (2003a), Characteristics of clathrate hydrate equilibria in mesopores and interpretation of experimental data, *J. Phys. Chem. B.*, *107*, 3500–3506.

Anderson, R., M. Llamedo, B. Tohidi, and R. W. Burgass (2003b), Experimental measurement of methane and carbon dioxide clathrate hydrate equilibria in mesoporous silica, *J. Phys. Chem. B*, *107*, 3507–3514.

Aya, I., K. Yamane, and H. Nariai (1997), Solubility of $CO_2$ and density of $CO_2$ hydrate at 30 MPa, *Energy*, *22*, 263–271.

Birchwood, R., S. Noeth, and P. Hooyman (2005), Wellbore stability model for marine sediments containing gas hydrates, paper presented at AADE 2005 National Technical Conference and Exhibition, Am. Assoc. of Drill. Eng., Houston, Tex.

Briaud, J. L., and A. Chaouch (1997), Hydrate melting in soil around hot conductor, *J. Geotech. Geoenviron. Eng.*, *123*, 645–653.

Christenson, H. K. (2001), Confinement effects on freezing and melting, *J. Phys. Condens. Matter*, *13*, R95–R133.

Circone, S., S. H. Kirby, and L. A. Stern (2005a), Thermal regulation of methane hydrate dissociation: Implications for gas production models, *Energy Fuels*, *19*, 2357–2363.

Circone, S., S. H. Kirby, and L. A. Stern (2005b), Direct measurement of methane hydrate composition along the hydrate equilibrium boundary, *J. Phys. Chem. B*, *109*, 9468–9475.

Clennell, M., M. Hovland, J. S. Booth, P. Henry, and W. J. Winters (1999), Formation of natural gas hydrates in marine sediments: 1. Conceptual model of gas hydrate growth conditioned by host sediment properties, *J. Geophys. Res.*, *104*, 22,985–23,003.

Davie, M. K., O. Y. Zatsepina, and B. A. Buffett (2004), Methane solubility in marine hydrate environments, *Mar. Geol.*, *203*, 177–184.

Dillon, W. P., and M. D. Max (2000), Oceanic gas hydrate, in *Natural Gas Hydrate in Oceanic and Permafrost Environments*, edited by M. D. Max, pp. 61–76, Kluwer Acad., New York.

Duan, Z. H., and S. D. Mao (2006), A thermodynamic model for calculating methane solubility, density and gas phase composition of methane-bearing aqueous fluids from 273 to 523 K and from 1 to 2000 bar, *Geochim. Cosmochim. Acta*, *70*, 3369–3386.

Everett, D. H. (1961), Thermodynamics of frost damage to porous solids, *Trans. Faraday Soc.*, *57*, 1541–1551.

Handa, Y. P. (1990), Effect of hydrostatic pressure and salinity on the stability of gas hydrates, *J. Phys. Chem.*, *94*, 2652–2657.

Handa, Y. P., and D. Stupin (1992), Thermodynamic properties and dissociation characteristics of methane and propane hydrates in 70–Angstrom-radius silica-gel pores, *J. Phys. Chem.*, *96*, 8599–8603.

Holder, G. D., V. A. Kamath, and S. P. Godbole (1984), The potential of natural gas hydrates as an energy resource, *Annu. Rev. Energy*, *9*, 427–445.

Jallut, C., J. Lenoir, C. Bardot, and C. Eyraud (1992), Thermoporometry—Modeling and simulation of a mesoporous solid, *J. Membr. Sci.*, *68*, 271–282.

Kayen, R. E., and H. J. Lee (1991), Pleistocene slope instability of gas hydrate-laden sediment on the Beaufort sea margin, *Mar. Geotechnol.*, *10*, 125–141.

Kim, H. C., P. R. Bishnoi, R. A. Heidemann, and S. S. H. Rizvi (1987), Kinetics of methane hydrate decomposition, *Chem. Eng. Sci.*, *42*, 1645–1653.

Kuhs, W. F., G. Genov, D. K. Staykova, and T. Hansen (2004), Ice perfection and onset of anomalous preservation of gas hydrates, *Phys. Chem. Chem. Phys.*, *6*, 4917–4920.

Lide, D. R. (1997), *CRC Handbook of Chemistry and Physics*, 78th ed., 8–81 pp., CRC Press, Boca Raton, Fla.

Liu, X. L., and P. B. Flemings (2006), Passing gas through the hydrate stability zone at southern Hydrate Ridge, offshore Oregon, *Earth Planet. Sci. Lett.*, *241*, 211–226.

Marshall, D. R., S. Saito, and R. Kobayashi (1964), Hydrates at high pressures: Part 1. Methane-water, argon-water, and nitrogen-water systems, *AIChE. J.*, *10*, 202–205.

Moridis, G. J. (2003), Numerical studies of gas production from methane hydrates, *SPE J.*, *32*(8), 359–370.

Moridis, G. J., and E. D. Sloan (2006), Gas production potential of disperse low-saturation hydrate accumulations in oceanic sediments, U.S. Dept. of Energy, *Rep. LBNL 61446*, Washington, D. C.

Nixon, M. F., and J. L. H. Grozic (2007), Submarine slope failure due to gas hydrate dissociation: A preliminary quantification, *Can. Geotech. J.*, *44*, 314–325.

Osegovic, J. P., S. R. Tatro, and S. A. Holman (2006), Physical chemical characteristics of natural gas hydrate, in *Economic Geology of Natural Gas Hydrate*, edited by M. D. Max, A. H. Johnson, and W. P. Dillon, pp. 45–104, Springer, New York.

Pawar, R. J., G. A. Zyvoloski, N. Tenma, Y. Sakaoto, and T. Komai (2005), Numerical simulation of gas production from methane hydrate reservoirs, paper presented at Fifth International Conference on Gas Hydrates, Statoil, Trondheim, Norway, 12–16 June.

Santamarina, J. C., K. A. Klein, and M. A. Fam (2001), *Soils and Waves*, John Wiley, London.

Schroeter, J. P., R. Kobayashi, and M. A. Hildebrand (1983), Hydrate decomposition conditions in the system H2S-methane-propane, *Ind. Eng. Chem. Fundam.*, *22*, 361–364.

Servio, P., and P. Englezos (2001), Effect of temperature and pressure on the solubility of carbon dioxide in water in the presence of gas hydrate, *Fluid Phase Equilib.*, *190*, 127–134.

Sloan, E. D. (1998), *Clathrate Hydrates of Natural Gas*, 2nd ed., Marcel Dekker, New York.

Stern, L. A., S. Circone, S. H. Kirby, and W. B. Durham (2001), Anomalous preservation of pure methane hydrate at 1 atm, *J. Phys. Chem. B*, *105*, 1756–1762.

Sultan, N. (2007), Comment on ''Excess pore pressure resulting from methane hydrate dissociation in marine sediments: A theoretical approach" by Wenyue Xu and Leonid N. Germanovich, *J. Geophys. Res.*, *112*, B02103, doi:10.1029/2006JB004527.

Sultan, N., P. Cochonat, J. P. Foucher, and J. Mienert (2004), Effect of gas hydrates melting on seafloor slope instability, *Mar. Geol.*, *213*, 379–401.

Sultan, N., M. Voisset, T. Marsset, A. M. Vernant, E. Cauquil, J. L. Colliat, and V. Curinier (2007), Detection of free gas and gas hydrate based on 3D seismic data and cone penetration testing: An example from the Nigerian Continental Slope, *Mar. Geol.*, *240*, 235–255.

Uchida, T., T. Ebinuma, and T. Ishizaki (1999), Dissociation condition measurements of methane hydrate in confined small pores of porous glass, *J. Phys. Chem. B*, *103*, 3659–3662.

Uchida, T., T. Ebinuma, S. Takeya, J. Nagao, and H. Narita (2002), Effects of pore sizes on dissociation temperatures and pressures of methane, carbon dioxide, and propane hydrates in porous media, *J. Phys. Chem. B*, *106*, 820–826.

Ullerich, J. W., M. S. Selim, and E. D. Sloan (1987), Theory and measurement of hydrate dissociation, *AIChE J.*, *33*, 747–752.

Williams, P. J., and M. W. Smith (1989), *The Frozen Earth—Fundamentals of Geocryology*, pp. 185–193, Cambridge Univ. Press., Cambridge, U. K.

Xu, W., and L. N. Germanovich (2006), Excess pore pressure resulting from methane hydrate dissociation in marine sediments: A theoretical approach, *J. Geophys. Res.*, *111*, B01104, doi:10.1029/2004JB003600.

Xu, W., and L. N. Germanovich (2007), Reply to comment by Nabil Sultan on ''Excess pore pressure resulting from methane hydrate dissociation in marine sediments: A theoretical approach,'' *J. Geophys. Res.*, *112*, B02104, doi:10.1029/2006JB004722.